Appl. Phys. A 80, 1641–1646 (2005)
DOI: 10.1007/s00339-004-3197-6

Applied Physics A
Materials Science & Processing

J. LEE[1]
W. GAO[2]
Z. LI[2]
M. HODGSON[2]
J. METSON[3,✉]
H. GONG[4]
U. PAL[5]

Sputtered deposited nanocrystalline ZnO films: A correlation between electrical, optical and microstructural properties

[1] Department of Mechanical Engineering, The University of Auckland, Private Bag 92019, Auckland, New Zealand
[2] Department of Chemical and Materials Engineering, The University of Auckland, Private Bag 92019, Auckland, New Zealand
[3] Department of Chemistry, The University of Auckland, Private Bag 92019, Auckland, New Zealand
[4] Department of Materials Science, National University of Singapore, Singapore
[5] Instituto de Física, Universidad Autónoma de Puebla, Apdo. Postal J-48, Puebla, Pue. 72570, México

Received: 6 July 2004/Accepted: 14 December 2004
Published online: 2 March 2005 •

ABSTRACT Zinc oxide thin films were prepared by dc (direct current) and rf (radio frequency) magnetron sputtering on glass substrates. ZnO films produced by dc sputtering have a high resistance, while the films produced using rf sputtering are significantly more conductive. While the conductive films have a compact nodular surface morphology, the resistive films have a relatively porous surface with columnar structures in cross section. Compared to the dc sputtered films, rf sputtered films have a microstructure with smaller *d* spacing, lower internal stress, higher band gap energy and higher density. Dependence of conductivity on the deposition technique and the resulting *d* spacing, stress, density, band gap, film thickness and Al doping are discussed. Correlations between the electrical conductivity, microstructural parameters and optical properties of the films have been made.

PACS 73.25.+i; 81.15.cd; 81.05.ys

1 Introduction

Zinc oxide (ZnO) is a wide band gap (~ 3.3 eV) semiconductor with a hexagonal wurtzite structure. Thin films of ZnO are of great interest because of their low toxicity, potential applications as transparent electrodes, solar cell windows, phosphors, gas sensors, surface acoustic wave devices and piezoelectric actuators. Recent success in producing large-area single crystals has opened up the possibility of using ZnO to produce blue and UV light emitters, and high-temperature, high-power transistors [1, 2]. The use of ZnO blue lasers in a CD writer could increase the amount of data storage by four times [3]. However, the electrical properties of ZnO are difficult to control. Reported resistivity of ZnO or Al doped ZnO thin films prepared by magnetron sputtering are in the range of 10^{-4} to 10^{5} Ω cm [4, 5]. Generally, Zn-rich defects such as zinc interstitials (Zn_i) and oxygen vacancies (V_O) are believed to be the main source of conductivity in as grown ZnO [6, 7] samples. The effect of several parameters like film thickness, grain and agglomerate size, grain boundary and impurity on the electrical property of ZnO thin films have been reported [8–11]. However, there are not many reports addressing the effect of microstructure on optical and electrical properties of ZnO thin films.

Magnetron sputtering is a popular technique to prepare thin films. In this paper we report the results of a detailed study of the electrical, optical and microstructural parameters of dc and rf sputtered undoped and Al doped ZnO thin films. We tried to correlate these parameters which might be useful for preparing ZnO thin films of desired characteristic through sputtering technique.

2 Experimental

A series of ZnO films were deposited by dc and rf magnetron sputtering using direct and reactive sputtering modes. Argon and argon-oxygen mixtures were used as the plasma-forming gas. Working pressure in the chamber was varied from 2 to 20 mTorr keeping the cathode-to-substrate distance 13 cm and deposition time 1–4 h. The sputtering targets were ZnO (99.9%) or Zn (99.99%), with an Al thin strip attached on the surface of the target for Al doping. Microscopic glass slides were used as substrates, which were in rotation during deposition. ZnO thin films were deposited at various deposition conditions as listed in Table 1. The electrical resistivity of the films was measured by standard two-probe and four-probe techniques. Scanning electron microscopy (SEM, Philips XL-30S with analytical system attached) and X-ray diffractometry (XRD, Bruker D8) were used to characterize the microstructure of the films. A surface profilometer (DEKTAK II) was used for thickness measurement of the films. Hall coefficients of the samples were measured at room temperature by an automized dc Hall measurement system using the Van Der Pauw technique. A HP 8254 spectrophotometer was used for recording the optical transmission spectra of the samples in the 190–800 nm spectral range.

3 Results

The XRD patterns of the ZnO films are shown in Fig. 1. The spectra revealed only strong (002) and weak (004) peaks, indicating a strong preferred orientation perpendicular to the substrate. As the surface energy density of the (002)

✉ Fax: +64-9-373-7925, E-mail: j.metson@auckland.ac.nz

No.	P mTorr	Power	Bias V dc	Time	Target	Thick-ness nm	Resist-ivity Ω cm	Band gap eV	X-ray density g/cm^3	d spacing nm	Stress GPa
Z-16	10.0/Ar	0.25A/dc	−50.0	4.0 h	ZnO	1240	1.0×10^6	3.09	5.650	0.2614	−1.0758
Z-17	20.0/Ar	0.25A/dc	−50.0	4.0 h	ZnO	954	9.7×10^5	3.12	5.650	0.2614	−1.0570
Z-25	20.0/Ar	0.25A/dc	−150.0	4.0 h	ZnO	1598	5.0×10^5	3.09	5.649	0.2614	−1.1066
Z-22	20.0/Ar	125W/rf	0	4.0 h	ZnO	675	0.160	3.20	5.661	0.2609	−0.5786
Z-19	20.0/Ar	125W/rf	−50.0	4.0 h	ZnO	576	1.060	3.19	5.664	0.2608	−0.4446
Z-20	10.0/Ar	125W/rf	−50.0	4.0 h	ZnO	681	0.031	3.17	5.666	0.2607	−0.3672
Z-21	20.0/Ar	250W/rf	−50.0	40 min	ZnO	417	0.010	3.20	5.668	0.2606	−0.2372
Z-23	10.0/Ar	250W/rf	−50.0	1.0 h	ZnO	464	0.009	3.16	5.664	0.2607	−0.4128
Z-36	2.0/Ar:O_2 = 6 : 4	0.25A/dc	−50.0	2.0 h	Zn + Al	437	2.7×10^6	3.08	5.601	0.2637	−3.3554
Z-37	2.0/Ar:O_2 = 6 : 4	0.25A/dc	−100.0	2.0 h	Zn + Al	437	2.1×10^6	3.11	5.602	0.2636	−3.2830
Z-38	2.0/Ar:O_2 = 6 : 4	0.25A/dc	0	2.0 h	Zn + Al	456	1.03×10^6	3.14	5.612	0.2632	−2.8572
Z-43	10.0/Ar:O_2 = 9 : 1	250W/rf	−50.0	2.0 h	Zn + Al	267	1.19	3.23	5.666	0.2606	−0.3216
Z-44	10.0/Ar:O_2 = 9 : 1	250W/rf	0	2.0 h	Zn + Al	337	0.137	3.29	5.669	0.2605	−0.2094
Z-45	10.0/Ar:O_2 = 9 : 1	250W/rf	−100.0	2.0 h	Zn + Al	315	3.69	3.24	5.671	0.2604	−0.1201
Z-46	10.0/Ar:O_2 = 9 : 1	250W/rf	−50.0	2.0 h	Zn	300	763	3.22	5.659	0.2610	−0.6679

TABLE 1 Processing parameters and properties of some typical ZnO thin films deposited by magnetron sputtering

orientation is the lowest in a ZnO crystal, (002) orientation is favored in the film [12]. In most of the samples, estimated d_{002} values are higher than the standard d_{002} value for unstressed powder (0.26033 nm, ASTM [13]) suggesting an elongation of unit cells along the c axis, and existence of compressive stresses along the plane of the films.

To derive the stress σ_{film} parallel to the film surface, the following formula can be used for a hexagonal lattice [14]:

$$\sigma_{\text{film}} = \left[2C_{13}^2 - C_{33}(C_{11}+C_{12})\right](C_{\text{film}} - C_{\text{bulk}}) \,/\, (2C_{13}C_{\text{bulk}}) \tag{1}$$

where C_{ij} are the elastic constants, C_{film} and C_{bulk} are lattice constants of the film and bulk, respectively. C_{ij} data for single crystal ZnO have been used as $C_{11} = 208.8$ GPa, $C_{33} = 213.8$ GPa, $C_{12} = 119.7$ GPa and $C_{13} = 104.2$ GPa. This yields the following numerical relation for the stress derived from XRD results:

$$\sigma_{\text{film}} = -232.8\,(C_{\text{film}} - C_{\text{bulk}})\,/C_{\text{bulk}}\,. \tag{2}$$

The calculated d spacing and stress for the films are listed in Table 1. The negative estimated stress for the films indicates that the lattice constant c is elongated, as compared to the unstressed powder sample.

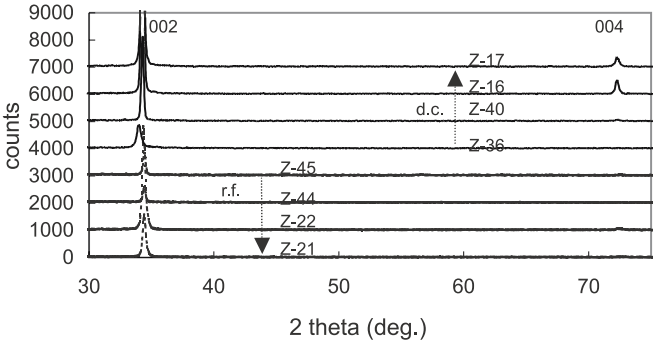

FIGURE 1 XRD spectra of dc sputtered and rf sputtered ZnO thin films

In order to estimate the density of a unit cell of ZnO thin film by X-ray analysis, we used the relation:

$$\text{X-ray density} = M/(NV) \tag{3}$$

where M is the total mass in a unit cell of ZnO; N, the Avogadro number, and V is the volume of the unit cell. Considering the bulk lattice parameter a value [13], we calculated the density for the films in the range of 5.602–5.671 g/cm^3, which is lower than the value for unstressed ZnO powder (5.674 g/cm^3). The error in the estimation of X-ray density was ±0.002 g/cm^3. Such a lower density of unit cells in our films is due to stress induced elongation of unit cells.

Typical surface and cross-sectional SEM micrographs of the ZnO films are shown in Fig. 2. From the micrographs we can observe the formation of nanometer size grains in the films with varying grain size for the films grown under different conditions. In general, the dc sputtered films grow along the c axis with a good columnar structure, where as, the rf sputtered films grow along c axis with shorter columnar structures and with slightly arbitrary orientation (Fig. 2b). The rf sputtered films reveal lower surface porosity than their dc counterparts (Fig. 2a).

Almost all the films prepared by dc sputtering from the ZnO target (Table 1) have resistivity higher than 10^5 Ω cm. Where as, all the films prepared by rf sputtering have lower resistivity (9.0×10^{-3}–7.63×10^2 Ω cm). In the case of reactive sputtering, while the doping of Al did not cause any substantial change in conductivity of the films prepared by dc process, the resistivity of the films decreased with Al doping (0.86%–1.65%) for the rf sputtered films. A similar decrease of resistivity in ZnO films is observed by Majumdar et al. [15] for < 4% Al doping in their chemical solution deposited films.

It is well known that the composition of thin films affect strongly their electrical conductivity [5, 6]. We performed energy dispersive spectroscopy (EDS) analysis of the samples but could not notice any gross variation in their compositions. Though the oxygen content in the samples varied from 41.8 at. % to 44.8 at. %, their resistivity varied from 9.0×10^{-3}–2.7×10^6 Ω cm, implying that not only the

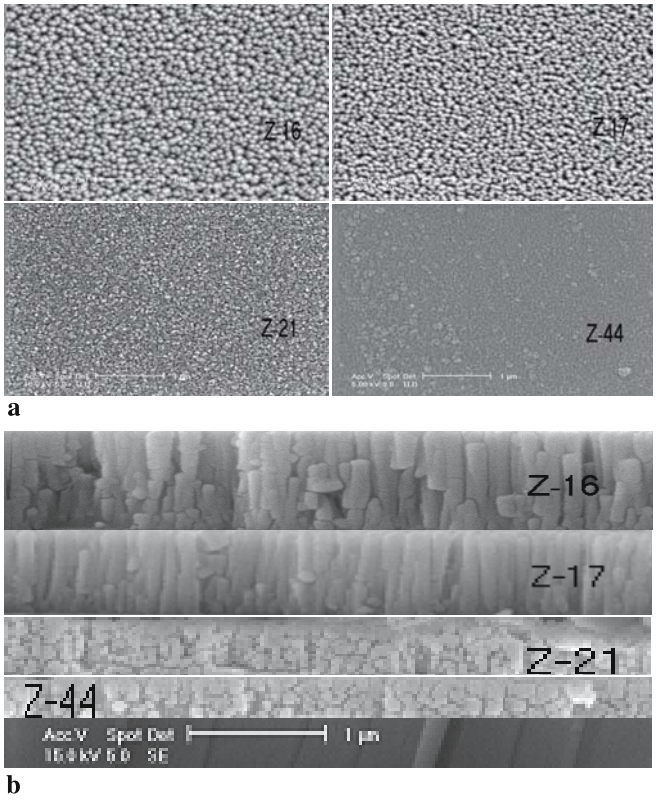

FIGURE 2 SEM micrographs of ZnO thin films: (**a**) top view, and (**b**) cross section. Samples Z-16 and Z-17 were prepared by dc sputtering; Z-21 and Z-44 were prepared by rf sputtering

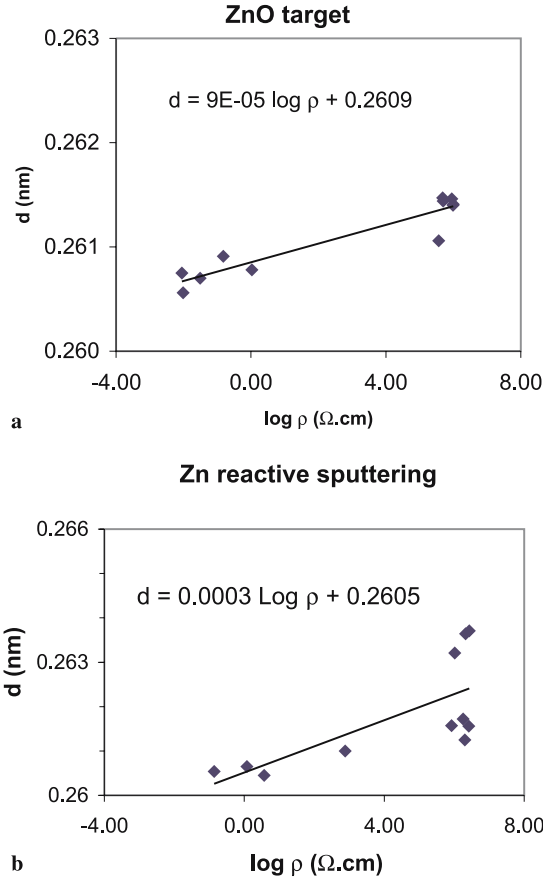

FIGURE 3 *d* spacing and resistivity relationship for ZnO thin films produced by direct (**a**) and reactive sputtering (**b**)

composition, but also other factors such as the microstructure have significant influences on the conductivity of the films.

From the Table 1, we can see that all ZnO films with good conductivity (samples with resistivity less than 10 Ω cm) have relatively small *d*spacing (< 0.261 nm), while the poorly conductive ZnO films (samples with resistivity > 500 Ω cm) have a larger *d* spacing (> 0.261 nm). Plots of log ϱ vs. *d* spacing for the films prepared with a ZnO target and through Zn reactive sputtering are shown in Fig. 3. Both the plots follow more or less a linear relationship. From the slopes of the linear fits, we could extract relationships between the resistivity and lattice spacing for the two cases. For the highly resistive films (> 10^4 Ω cm), the linear fits are not as good as for low resistivity films. Hence, the lattice spacing alone can't account for conductivity differences.

The results also show that the most conductive ZnO films have higher density (> 5.66 g/cm^3), while the poorer conducting films have lower density (< 5.66 g/cm^3). The log ϱ vs. X-ray density plots for the ZnO films are shown in Fig. 4. While the highly conductive films have absolute stress values less than 0.70 GPa, the poor-conductive films (resistivity higher than 10^3 Ω cm) have stress values higher than 0.72 Gpa (Table 1).

As the conductivity of the films depends on their thickness, we prepared several films with different deposition times to obtain films 150 to 675 nm thick. The log ϱ of the films decreased almost linearly with the increase of film thickness (Fig. 5) as observed by other workers [16]. However, similar

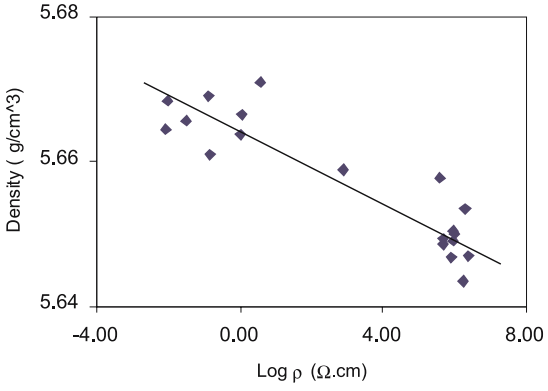

FIGURE 4 Variation of resistivity with X-ray density of ZnO thin films

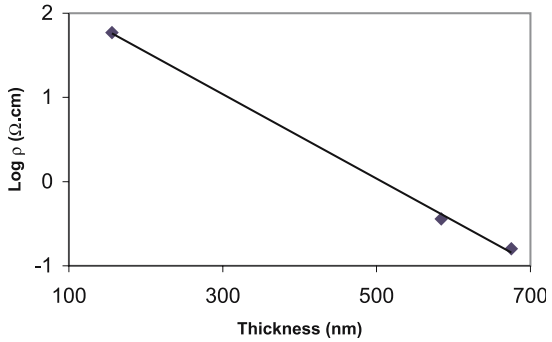

FIGURE 5 Variation of resistivity with film thickness for Z-22 series ZnO thin films

Sample	P	Power	Bias (V dc)	Target (Ω cm)	Resistivty (mTorr)	Mobility (cm^2/V)	Carrier conc. (cm^{-3})
Z-21	20.0/Ar	250W/rf	−50.0	ZnO	0.0097	13.7	2.00×10^{19}
Z-44	$10.0/Ar:O_2 = 9:1$	250W/rf	0	Zn + Al Reactive	0.137	0.287	6.00×10^{18}
Z-45	$10.0/Ar:O_2 = 9:1$	250W/rf	−100.0	Zn + Al Reactive	3.69	0.330	4.50×10^{17}

TABLE 2 Resistivity, mobility and carrier concentration data of selected ZnO films

behavior is not observed for the films prepared with different processing parameters.

All the doped and undoped films, prepared either by dc or rf sputtering show n-type conductivity which might be due to Zn excess (as determined from the EDS measurements) in them. From Table 2, we can see that the highly conductive film (sample Z-21, $\varrho = 0.0097\,\Omega$ cm) has a mobility of $13.7\,cm^2/V\,s$ and a carrier concentration of $2.0 \times 10^{19}\,/cm^3$. Whereas, a higher resistivity film (sample Z-45, $\varrho = 42.0\,\Omega$ cm) has a mobility of $0.33\,cm^2/V\,s$ and a carrier concentration of $4.517\,/cm^3$. Therefore, as expected the carrier concentration and the carrier mobility of the samples decreased with their conductivity.

To study the conduction mechanism in our undoped ZnO films, conductivity measurements were performed at different temperatures for the films prepared by dc and rf sputtering of ZnO targets. In Fig. 6 the plots of resistivity vs. temperature for the ZnO films prepared by rf sputtering (Fig. 6a) and dc sputtering (Fig. 6b) are shown. The calculated conductivity was found to follow the Arrhenious equation:

$$\sigma = \sigma_0 \exp(-E_a/kT) \tag{4}$$

where, σ_0 is a constant, E_a is the activation energy of the electron transport in the conduction band, k is the Boltzman constant and T is the temperature. Figure 6 shows two linear regions for both rf and dc sputtered ZnO films, revealing two activation energies, one for higher and one for the lower temperature ranges. The activation energies (E_{a1} and E_{a2}) calculated for the respective temperature ranges are shown in Fig. 6. The evaluated activation energies are in agreement with the values reported for sol–gel derived ZnO films [17].

The band gap energy of the films has been measured from the optical transmission spectra using the photon energy at half maximum absorption [18]. From the calculated values presented in Table 1, all the films produced by dc sputtering

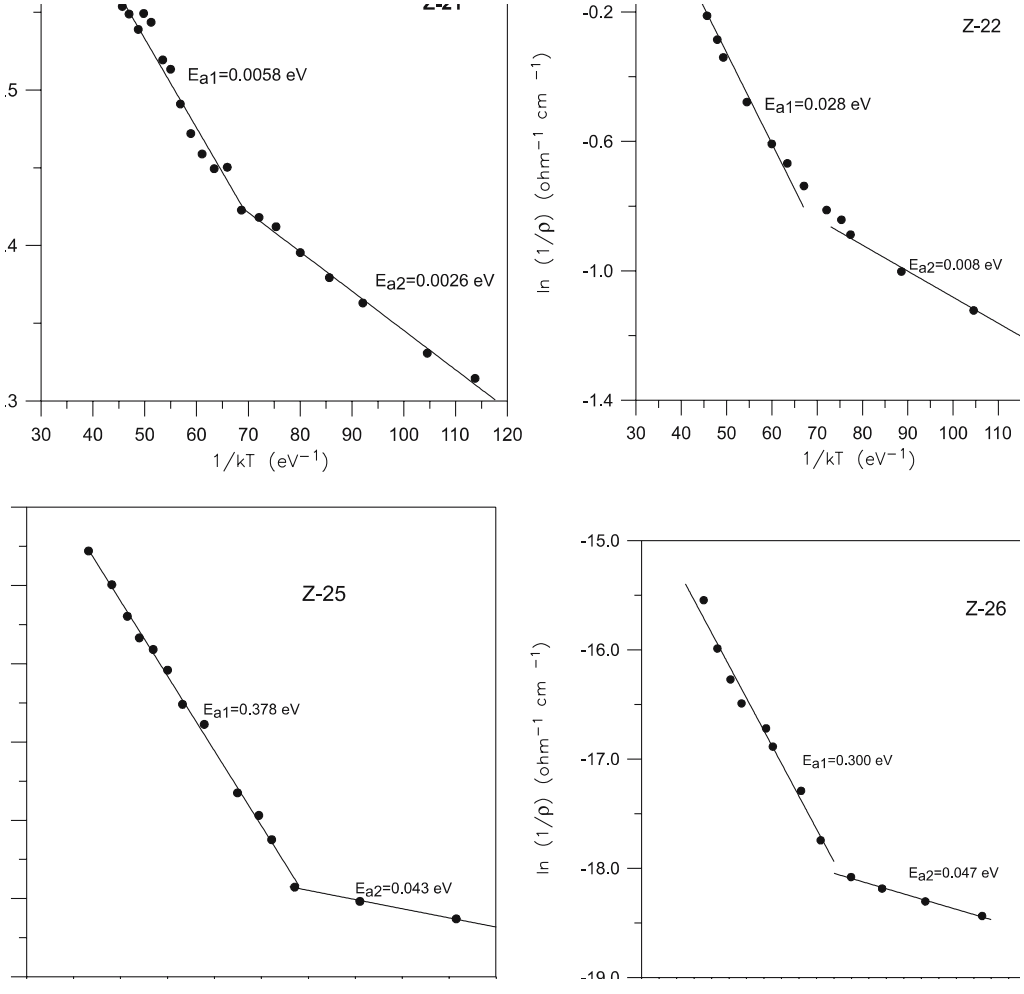

FIGURE 6 Variation of resistivity with temperature for (**a**) rf sputtered and (**b**) dc sputtered ZnO films

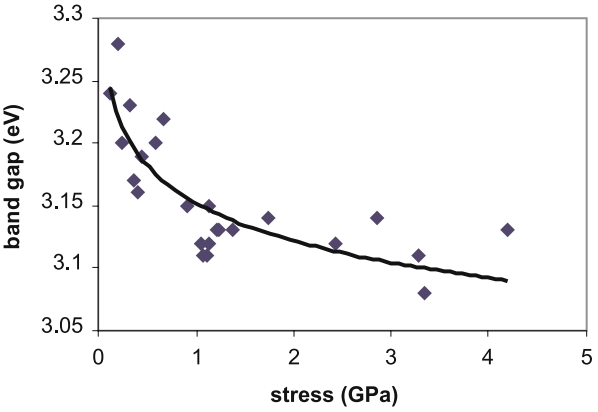

FIGURE 7 Variation of band gap of ZnO thin films with stress

show band gaps smaller than 3.15 eV; however, the band gaps of the films produced by rf sputtering are higher. As the residual stress can change the lattice spacing [19] and band gap (Fig. 7), we expect higher lattice constant c for the films grown by dc sputtering. The elongated c axis might decrease overlap between the atomic wave-functions, decreasing the separation between the conduction and valence bands [20] and therefore causing a decrease in band gap.

4 Discussion

Our results indicate that rf sputtered films have better conductivity than those produced by dc sputtering. In rf sputtering, breakdown ionization occurs by heating electrons in the gas plasma with a fluctuating field, an effect which is not present with a constant dc field. The main difference between dc and rf excitation is a much higher ion to neutral ratio (by a factor of 4–10) for the rf discharge, which is caused by a higher plasma density in front of the substrate and a lower deposition rate for the same discharge power. Thus, the ion bombardment can be achieved at a lower pressure with rf sputtering than dc sputtering. rf deposition leads to a more homogeneous distribution of grains. The lower resistivity of the rf sputtered films is attributed to their higher carrier concentration and higher carrier mobility. It is also suggested that the lower internal stresses in the rf sputtered films, caused by the better crystalline quality, leads to their higher carrier mobility [14]. However, in our samples, though the average crystallite size of the rf sputtered films is smaller than the average crystallite size of the dc sputtered films, the lower resistivity of the rf sputtered films is likely due to lower internal stress. Lower strain in the rf deposited films might be due to strain relaxation through breaking the columnar structures into smaller grains (Fig. 2).

Defects such as zinc interstitials (Zni) and oxygen vacancies (V_O) are commonly accepted as the main sources of conductivity in as grown films [6, 7]. The conductivity of these films comes from the stoichiometric deviations (oxygen vacancies and excess metal ions) [6]. The incorporation of the point and textured defects, however, might be one of the reasons for lower conductivity [20]. It is also thought that porosity contributes to their poor conductivity.

The resistivity of the rf sputtered ZnO films decreased on incorporation of Al probably due to the contribution of extra free carriers from Al^{+3} ions substituting Zn^{+2} ions. However, as the radius of Al atoms is smaller than the radius of Zn atoms, part of the incorporated Al may occupy interstitial positions in the ZnO lattice [21].

The conductivity (σ) is a combination of mobility μ and carrier concentrations n and can be written as:

$$\sigma = ne\mu\,. \tag{5}$$

The total mobility, μ, is represented as [23]:

$$1/\mu = 1/\mu_{\mathrm{L}} + 1/\mu_{\mathrm{i}} + 1/\mu_{\mathrm{g}} \tag{6}$$

where μ_{L} is the mobility due to the lattice scattering, μ_{i} and μ_{g} are the mobility due to the impurity scattering and grain boundary scattering, respectively.

Several reports [9, 10, 24] suggested that the Hall mobility of ZnO is influenced by ionized impurity scattering and grain boundary scattering. μ_{H} is expressed as:

$$1/\mu_{\mathrm{H}} = 1/\mu_{\mathrm{i}} + 1/\mu_{\mathrm{g}} \tag{7}$$

where μ_{i} and μ_{g} are the mobility due to the impurity scattering and grain boundary scattering, respectively. It is believed that the grain boundary scattering of charge carriers is predominant in the electrical conductivity of ZnO films [9, 10, 24]. Mobility is determined by both ionized impurity scattering and grain boundary scattering.

The effect of grain boundaries in the electrical properties is prominent when the grain size is small. XRD analysis and SEM observations revealed the average crystallite size in the rf sputtered and dc sputtered samples to be of the order of 35 nm and 82 nm, respectively. To interpret the conductivity behavior of ZnO thin films, we can assume that the resistivity of these films comes from grain boundary resistivity ϱ_{G}, lattice resistivity ϱ_{L}, impurity resistivity ϱ_{I} and porosity resistivity ϱ_{d}, i.e.:

$$\varrho = \varrho_{\mathrm{G}} + \varrho_{\mathrm{L}} + \varrho_{\mathrm{I}} + \varrho_{\mathrm{d}} \tag{8}$$

or

$$1/\sigma = 1/\sigma_{\mathrm{G}} + 1/\sigma_{\mathrm{L}} + 1/\sigma_{\mathrm{I}} + 1/\sigma_{d} \tag{9}$$

where σ is the respective conductivity. Equation (9) assumes that the resistance from grain boundaries, lattice, impurities and pores can be put in a series.

The grain boundary conduction plays an important role in the conductivity of thin films because of the very small grain sizes. The grain boundary barrier depends on the microvoids, inter-grain distance, grain size, impurity concentration, crystallinity, and non coordinated atoms at the grain boundaries [8, 25]. In the rf sputtered undoped ZnO films, we obtained activation energy values (0.028 and 0.0058 eV for E_{a1}; 0.008 and 0.0026 eV for E_{a2}) considerably smaller than the values (0.378 and 0.300 eV for E_{a1}; 0.047 and 0.043 eV for E_{a2}) for dc sputtered films. While the activation energy at higher temperatures is derived from charge transport in the conduction band, the lower energy activation energy is derived from electronic hoping between the nearest neighbors (donors) [17]. We can see that both the transition temperature

and activation energy are different for the ZnO films prepared by rf and dc sputtering. We believe that the changes are due to the difference in grain size in the films. A lower grain side in the rf sputtered films induces a lower temperature transition in conduction mechanism (i.e., from hopping conduction to band type conduction).

The effects of film thickness on the electrical conductivity are complex. The results obtained from limited samples show that the conductivity of the films increased with increasing thickness. The increased thickness or crystal size weakens the inter-crystallite boundary scattering and increases the carrier lifetime, consequently, increasing the mobility of carriers [8]. However, the porosity of the films may also play an important role in their conductivity.

ZnO is an ionic crystal, with binding determined mostly by the Madelung energy due to the long range of Coulomb interaction. Smaller inter-atomic spacing will open up the fundamental gap and will stretch the electronic spectrum due to the increased overlap between atomic wavefunctions, which we believe is responsible for the higher band gap in rf sputtered films.

An increase in band gap by Al doping is observed in the rf sputtered ZnO films while their electrical conductivity increased. The shift of the absorption edge to higher energy in the Al doped films can be attributed to the increase in carrier concentration of the Fermi level and blocking of energy transitions, causing a Burstein Moss effect [12, 26, 27].

5 Conclusions

Zinc oxide thin films were prepared by dc and rf magnetron sputtering on glass substrates. The electrical conductivity of the films has been studied in relation to the microstructure and optical properties. Most of the ZnO films produced by dc sputtering have a high resistance, while the films produced by rf sputtering are significantly more conductive. The band gap energies of the ZnO films prepared by dc sputtering are smaller than the films prepared by rf sputtering. While the highly conductive films have a nodular and compact surface texture, the poorly conducting films grow with columnar grains and porous surface texture. Compared to dc, rf deposition leads to the formation of ZnO films with more homogeneous microstructure, smaller d spacing, higher calculated X-ray density and lower internal stress. The electrical conductivity of ZnO films follows a linear relationship with their d spacing, stress, density and thickness. Incorporation of Al in low concentration ($< 2\%$) mainly causes substitution for Zn in the ZnO lattice thereby reducing its resistivity. The conduction mechanism in sputtered n-type ZnO films is controlled through the charge transport in the conduction band and electronic hoping between the nearest neighbor donor levels. The electrical conductivity of sputtered ZnO thin films is affected by many factors including film processing, composition and microstructure. A good understanding of these parameters is necessary to improve the electrical conductivity of ZnO films for industrial applications.

ACKNOWLEDGEMENTS The work is partially supported by Marsden Fund, the Royal Society of New Zealand. J. Lee would like to thank New Zealand Foundation for Research, Science and Technology for a Bright Futures Scholarship, and the Australian Institute of Nuclear Science and Engineering for a postgraduate award. We acknowledge Drs. A. Asadov, T. Ashida, P. Schwerdtfeger and D. Tomanek for helpful discussions.

REFERENCES

1 D.C. Look: Mater. Sci. Eng., B **80**, 383 (2001)
2 R. Ondo-Ndong, F. Pascal-Delannoy, A. Boyer, A. Giani, A. Foucaran: Mater. Sci. Eng., B **97**, 68 (2003)
3 R.F. Service: Science **276**, 895 (1997)
4 A.V.F. Quaranta, F.R. Rizzi, G. Casamassima: J. Appl. Phys. **74**, 244 (1993)
5 G.J. Fang, D. Li, B.L. Yao: Thin Solid Films **418**, 156 (2002)
6 F.J. Haug, Z.S. Geller, H. Zogg, A.N. Tiwari, C. Vignali: J. Vac. Sci. Technol. A **19**, 171 (2001)
7 S. Dogan, A. Ates, G. Xiong, J. Wilkinson, S. Tuzemen, M. Yildirim, R.T. Williams: Phys. Status Solidi A **195**, 165 (2003)
8 X.T. Hao, J. Ma, D.H. Zhang, T.L. Yang, H.L. Ma, Y.G. Yang, C.F. Cheng, H. Huang: Appl. Surf. Sci. **189**, 18 (2002)
9 K.C. Park, D.Y. Ma, K.H. Kim: J. Appl. Phys. **81**, 7764 (1997)
10 S. Uthanna, T.K. Subramanyam, B.S. Naidu, G.M. Rao: Opt. Mater. **19**, 461 (2002)
11 Z. Ji, C. Yang, K. Liu, Z.Z. Ye: J. Cryst. Growth **253**, 239 (2003)
12 M.K. Jayaraj, A. Antony, M. Ramachandran: Bull. Mater. Sci. **25**, 227 (2002)
13 V. Gupta, A. Mansingh: J. Appl. Phys. **80**, 1063 (1996)
14 R. Cebulla, R. Wendt, K. Ellmer: J. Appl. Phys. **83**, 1087 (1998)
15 S.B. Majumdar, M. Jain, P.S. Dobal, R.S. Katiyar: Mater. Sci. Eng., B **103**, 16 (2003)
16 M. Izaki, H. Ishizaki, A. Ashida, T. Omi, T. Ito: J. Jap. Inst. Met. **62**, 1063 (1998)
17 Y. Natsume, H. Sakata: Thin Solid Films **372**, 30 (2000)
18 S.A. Studenikin, N. Golego, M. Cocivera: J. Appl. Phys. **83**, 2104 (1998)
19 O. Takai, M. Futsuhara, G. Shimizu, C.P. Lungu, J. Nozue: Thin Solid Films **318**, 117 (1998)
20 W.S.J. Bardeen: Phys. Rev. **80**, 72 (1950)
21 D. Cossemet, J.M. Streydio: J. Cryst. Growth **72**, 57 (1985)
22 W. Tang, D.C. Cameron: Thin Solid Films **238**, 83 (1994)
23 Y. Natsume, H. Sakata: Mater. Chem. Phys. **78**, 170 (2003)
24 X.L. Xu, S.P. Lau, J.S. Chen, Z. Sun, B.K. Tay, J.W. Chai: Mater. Sci. Semicond. Process **4**, 617 (2001)
25 S. Surthi, S. Kotru, R.K. Pandey: Mater. Lett. **57**, 887 (2002)
26 H. Gomez, A. Maldonado, R. Asomoza, E.P. Zironi, J. Canetasortega, J. Palaciosgomez: Thin Solid Films **293**, 117 (1997)
27 D.H. Zhang, R.W. Gao, H.L. Ma: Thin Solid Films **295**, 83 (1997)